quaternary

MDPI

Article

Local Differentiation in the Loess Deposition as a Function of Dust Source: Key Study Novo Orahovo Loess Paleosol Sequence (Vojvodina, Serbia)

Slobodan B. Marković [1,2,*], Jef Vandenberghe [3], Zoran M. Perić [4], Dávid Filyó [5], Tamás Bartyik [5], Milica G. Radaković [1], Qingzhen Hao [6], Rastko S. Marković [7], Tin Lukić [1], Nemanja Tomić [1], Milivoj B. Gavrilov [1], Aleksandar Antić [1], Ivana Cvijanović [8] and György Sipos [5]

1 Department of Geography, Tourism and Hotel Management, Faculty of Science, University of Novi Sad, Trg Dositeja Obradovića 3, 21000 Novi Sad, Serbia
2 Serbian Academy of Arts and Sciences, Knez Mihailova 35, 11000 Belgrade, Serbia
3 Department of Earth Sciences, Vrije Universiteit Amsterdam, De Boelelaan 1085, 1081 HV Amsterdam, The Netherlands
4 Lund Luminescence Laboratory, Department of Geology, Lund University, Sölvegatan 12, SE-223 62 Lund, Sweden
5 Department of Physical Geography, University of Szeged, Egyetemut 2-6, H-6720 Szeged, Hungary
6 Key Laboratory of Cenozoic Geology and Environment, Institute of Geology and Geophysics, Chinese Academy of Sciences, Beijing 100029, China
7 Department of Geography and Tourism, Natural Sciences and Mathematics, University of Niš, 18000 Niš, Serbia
8 ISGlobal—Barcelona Institute for Global Health, 08036 Barcelona, Spain
* Correspondence: slobodan.markovic@dgt.uns.ac.rs or baca.markovic@gmail.com

Abstract: Typical patterns of the Late Pleistocene loess–paleosol units are preserved in the Novo Orahovo brickyard, Northern Serbia. Presented preliminary luminescence chronology supports the chronostratigraphic interpretations of global isotopic marine climate reconstructions. Magnetic susceptibility and sedimentological evidence exhibit general similarities with the marine oxygen-isotope stratigraphy. These records provide new insights into the dust accumulation regimes over the eastern side of the Bačka loess plateau and offer new paleoenvironmental information for the region. They represent an important step forward towards the establishment of a catena from the thin loess-like sediments of the Banat foothills in the east towards the thicker and seemingly more complete loess sections of the southeastern and central Carpathian Basin. Grain-size data from the loess record of Nova Orahovo explain the regional differentiation in dust deposition.

Keywords: Serbia; Late Pleistocene; loess; paleoclimate; paleoenvironment; regional dust variability

check for updates

Citation: Marković, S.B.; Vandenberghe, J.; Perić, Z.M.; Filyó, D.; Bartyik, T.; Radaković, M.G.; Hao, Q.; Marković, R.S.; Lukić, T.; Tomić, N.; et al. Local Differentiation in the Loess Deposition as a Function of Dust Source: Key Study Novo Orahovo Loess Paleosol Sequence (Vojvodina, Serbia). *Quaternary* **2023**, *6*, 23. https://doi.org/10.3390/quat6010023

Academic Editor: David J. Lowe

Received: 13 January 2023
Revised: 8 March 2023
Accepted: 11 March 2023
Published: 16 March 2023

1. Introduction

During the past two decades, loess–paleosol sequences located in the southeastern part of the Carpathian Basin have been intensively investigated due to their potential to provide deeper understanding of the regional Pleistocene climate and environmental dynamics in the region [1–16].

During the Late Pleistocene period, this area was an environmental transitional zone by the alternation of diverse ecotones ranging from dry-steppic to forest-steppic environments [17–21]. Loess has been deposited mostly during the formation of different types of grassland environments [22,23]. This significantly contrasts the paleoclimatic and paleoenvironmental reconstructions from other parts of the European loess belt, where loess is usually formed in a periglacial, or tundra–steppe, environment [24–31].

Despite the recent extensive investigations in the southeastern part of the Carpathian Basin [1–3,6,9], some local-to-regional elements of the Late Pleistocene environmental

dynamics still remain unresolved. To fill these gaps related to the last glacial environmental reconstructions of that region, we investigated the Novo Orahovo (Vojvodina, Serbia) loess section. We present the preliminary absolute luminescence chronology, magnetic, and sedimentological records of the Late Pleistocene climate and environment variations from the Novo Orahovo loess–paleosol sequence, located on the interfluve area between the Danube and Tisa (Tisza) rivers at the Bačka loess plateau (LP) in Northern Serbia (Figure 1).

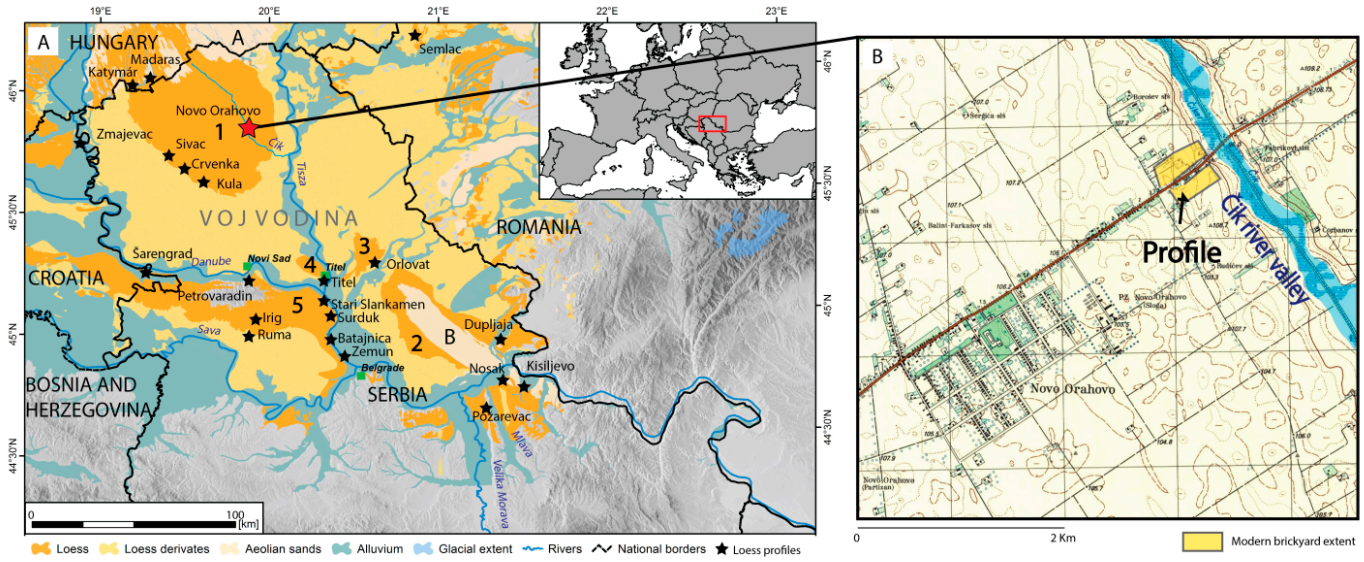

Figure 1. Distribution of the loess sediments and loess derivates in the southeastern Carpathian Basin with the position of the Novo Orahovo loess section and other key loess sites in the region. Distribution of loess, loess derivates, aeolian sand, and alluvium according to Lehmkuhl et al. (2018) [10] and JAXA EORC (2016) [11], respectively. Loess plateaus (LP): 1. Bačka LP; 2. Banat LP; 3. Tamiš LP; 4. Titel LP; 5. Srem LP. Sandy terrains (ST): (**A**) Bačka ST; (**B**) Banat ST. Modified after Perić et al. (2022) [12].

2. Material and Methods

The Novo Orahovo brickyard is situated in Northern Serbia (latitude N 45°51′55″ and longitude E 19°48′01″) in the Bačka LP, between the alluvial plains of the Danube and Tisa rivers. The investigations of the loess–paleosol sequences at the Novo Orahovo quarry began in 2017. After careful cleaning and a detailed description of the investigated sections, samples were collected for color determination, magnetic susceptibility (MS), and grain-size analysis and luminescence dating. Dry and moist colors of the loess and paleosol units were characterized using Munsell Soil Color Charts. Bulk sediment samples were collected at 5 cm intervals for texture analysis.

The MS was measured using a Bartington MS2 B Dual Frequency Sensor instrument–36 mm sample cavity diameter, at the Laboratory of Physical Geography, Faculty of Sciences, University of Novi Sad, Serbia. The samples were first placed in non-magnetic plastic boxes, after which they were carefully compressed with a non-magnetic plastic pusher. Before closing the box, cotton wool was placed to prevent any movement of the material during the measurement.

The grain-size (GS) distribution of samples was carried out on a Fritsch Analysette 22 MicroTec laser diffraction grain-sizer at the Department of Geoinformatics, Physical and Environmental Geography, University of Szeged. The device is equipped with a green (λ = 532 nm, p = 7 mW) and an infrared (λ = 940 nm, p = 9 mW) laser, and has a measurement range of 0.08–2000 µm. Sample preparation followed the procedures detailed in Kun et al. (2013) [32] and Serban et al. (2015) [33]. Furthermore, no chemical dispersion was applied to avoid the modifying effect of the dispersant on the measurements. A longer, 180 s ultrasonic pretreatment (f = 36 kHz, p = 60 W) was applied instead [30]. To generate

grain-size distribution curves, the laser diffraction data were processed according to the Mie optical theory, using the following parameters: refraction index of 1.52 and absorption index of 0.1 for the dispersed sample and refraction index of 1.33 for water [34]. Apart from specific characteristic grain-size ranges, we also calculated the U-ratio. The latter sedimentary proxy expresses the proportion of medium- and coarse-grained silt (44–16 μm) versus fine-sized silt (16–5.5 μm) [35]. It especially enables the elimination of potentially present pedogenic (mostly submicron) clay.

The samples for luminescence dating were obtained by hammering stainless steel tubes into the freshly cleaned profile. In total, 20 samples were collected. Here, we present the initial dating results of 5 quartz samples from the upper 610 cm of the profile. The inner material of the cylinders was used for equivalent dose measurements (conducted at the Luminescence Dating Laboratory, University of Szeged, Hungary) and the outer material (~2 cm) for the present water content and radionuclide activity determination. The preparation of samples was conducted according to standard laboratory techniques [36]. All procedures were tested in subdued yellow light conditions. Selected samples were wet sieved using 90, 63, and 40 μm sieves. The <40 μm fraction was placed into Atterberg settling cylinders to separate the 4–11 μm silt fraction. However, none of the samples contained a sufficient amount of fine silt for further processing; therefore, in a second run, the 11–20 μm medium silt fraction was separated. Carbonate and organics were removed by repeated treatment in 10% HCl and 10% H_2O_2, respectively. To isolate the quartz grains, a portion of the 11–20 μm fraction was immersed in 35% H_2SIF_6 for 10 days. Subsequently, the quartz grains were treated with 30% HCl to remove any remaining fluorides.

The equivalent dose (De) of samples was determined on a Risø DA-20 TL/OSL-type luminescence reader equipped with a 90SR/90Y β-source and an EMI ET9107-type photomultiplier [37]. Stimulation was carried out using a blue (470 ± 30 nm) LEDs set for 90% power release, while detection was made through a Hoya U-340 filter. Throughout the measurements, the single aliquot regeneration (SAR) protocol was applied [38,39]. Subsequently, preheat plateau and dose recovery tests were performed to identify the optimal measurement parameters and assess the reproducibility of measurements. Appropriate stimulation temperatures were determined using preheat plateau and dose recovery tests on sample 1141. The initial 0.4 s minus a late background subtraction from the last 30 s was used when plotting dose points.

Natural aliquots were first bleached using blue LEDs at room temperature for 100 s, followed by a 3000 s pause, and subsequently further bleached at room temperature for 100 s [38]. Finally, a laboratory β-dose of 50 Gy was administered to the bleached aliquots and measured using a SAR protocol in which the preheating temperature varied between 180 and 300 °C, while the cut-heat temperature was fixed at 160 °C.

During OSL measurements, optical stimulation was performed at 125 °C (heating rate: 5 °C/s) for 40 s. Standard rejection criteria were used to select aliquots that performed well during the SAR measurements [38]. Potential feldspar contamination of the quartz extracts was monitored by the IR/OSL depletion ratio, as proposed by Duller (2003) [40]. In the case of each sample, at least 24 aliquots were analyzed. Dose–response curves were fitted in each case using the single saturating exponential function. The α-value was directly determined by recovering known α doses with β regeneration measurements on aliquots that previously went through a SAR procedure [41]. A representative dose–response curve is presented in Figure 2b.

The environmental dose rate (D*) was determined using high-resolution, extended-range gamma-ray spectrometry (Canberra XtRaCoaxial Ge detector). Dry dose rates were calculated using the conversion factors of Liritzis et al. (2013) [42]. The alpha and beta attenuation factors were estimated using the calculations of Brennan et al. (1999) [43] and Brennan (1999) [44], respectively, with dose rate conversion factors obtained from Guérin et al. (2012) [45]. Uncertainties are based on the propagation, in quadrature, of individual errors for all measured quantities, which, if unknown, are recorded as 10%. The cosmic ray contribution to the total dose rate was calculated according to Prescott

and Hutton (1994) [46] for each sample as a function of depth, altitude, and geomagnetic latitude, assuming an uncertainty of 10%. The total dose rate was calculated using DRAC version 1.2 [47].

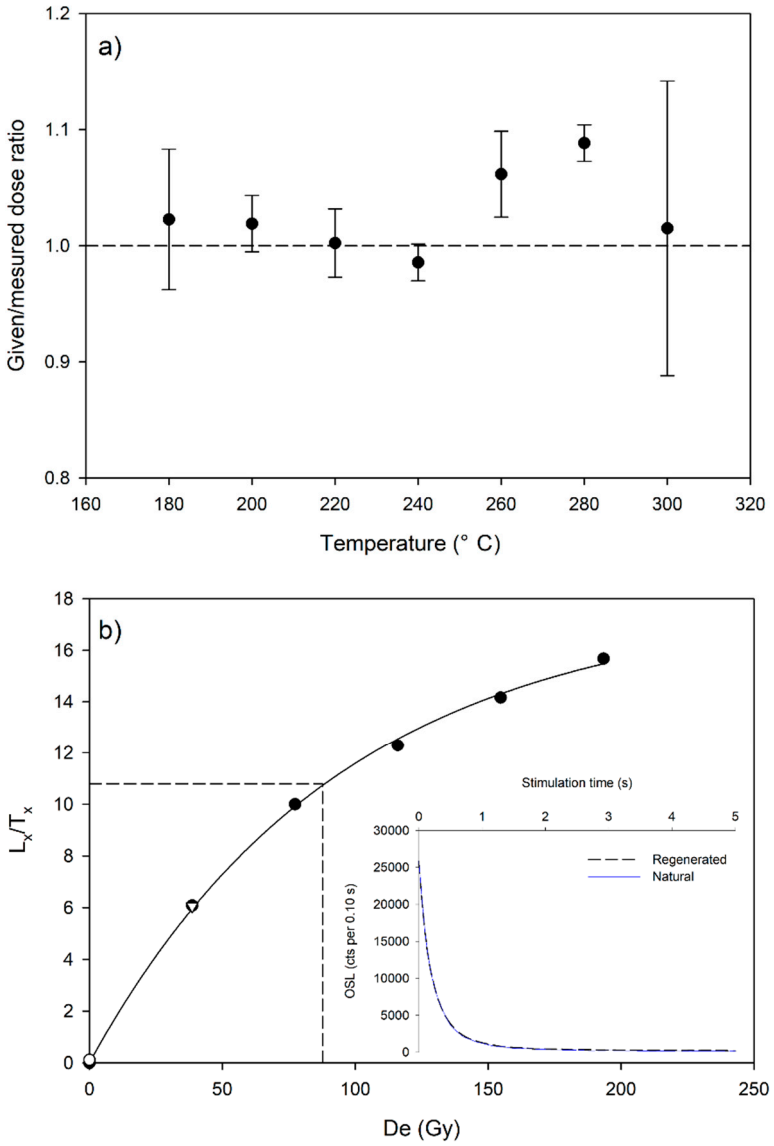

Figure 2. (**a**) Dose recovery ratio as a function of first preheat temperature for sample 1141. There were 3 aliquots used per preheat temperature and the error bars represent 1 standard error. The dashed line is drawn at an ideal ratio of 1.0. (**b**) Representative sensitivity-corrected dose–response curves for sample 1141. The dashed line shows the equivalent dose. The response to a zero dose is depicted as an open circle, while the recycling point is represented as an open inverted triangle. The inset displays a typical decay curve of natural CW-OSL (continuous-wave OSL signal) (full blue line) for the first 5 s of stimulation in comparison to a regenerated signal (dashed black line) induced by a beta dose approximately equal to the equivalent dose.

3. Results

3.1. Lithostratigraphy and Pedostratigraphy

The stratigraphic framework of loess–paleosol sequences from the Vojvodina region, Northern Serbia, is generally simple [2]. Aeolian dust deposition happened on a nearly horizontal platform of the Bačka LP, which exhibits a geomorphologically similar setting as that of the Chinese Loess Plateau [48–51]. Following the criteria presented by

Marković et al. (2015) [3], we describe, stratigraphically characterize, and label the loess and paleosol units at the Novo Orahovo loess section (see Figure 3 and Table 1).

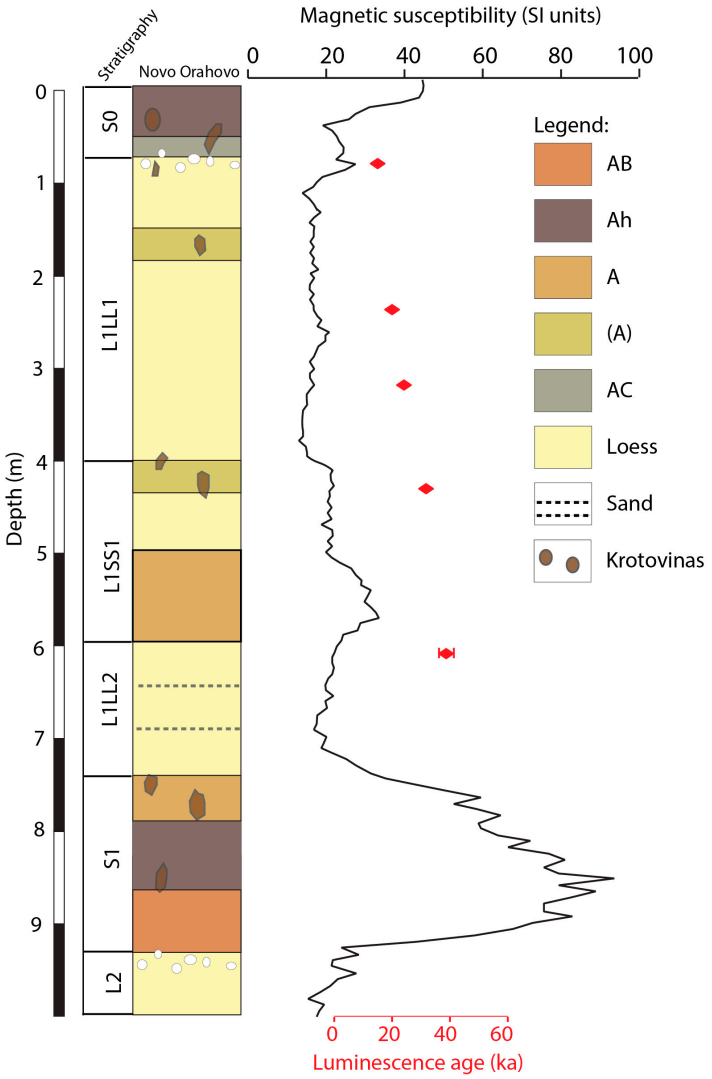

Figure 3. Magnetic susceptibility record (black line) and luminescence chronology (red dots) of the Novo Orahovo loess–paleosol sequence related to pedostratigraphy.

The uppermost part of the penultimate loess unit L2 is just 75 cm exposed in the lower part of its profile and correlates to the latest MIS 6. Many small carbonate spherical concretions (1–2 cm diameter) and humic infiltration in the former root channels were observed close to the contact with the overlaying paleosol S1 (developed during MIS 5). The last interglacial pedocomplex, S1, is 155 cm thick and shows a gradual decrease in pedogenic intensity over time. The 35 cm thick basal transitional AB horizon (10YR6/2–4) is strongly developed and characterized by a granular and partly blocky structure. Above this pedohorizon, two humic granular horizons Ah1 and Ah2 have been developed at a profile depth between 890 cm and 820 cm. Finally, the relatively weakly developed uppermost A horizon is 50 cm thick and strongly affected by numerous krotovinas. This pedogetic horizon represents a gradual weakening of pedogenesis and gently transforms into the overlaying thick loess unit L1. This last glacial composite loess unit is 680 cm thick in total. The lower loess subunit L1LL2 is 265 cm thick, porous, and represents a typical loess. It is interbedded by sandy layers, containing numerous krotovinas, and is in some parts bioturbated. The middle paleosol L1SS1 is developed at a profile depth between 515 cm and 450 cm. This is a slightly developed fossil chernozem-like paleosol (A horizon)

with intensive granular structure and krotovinas. The uppermost loess subunit L1LL1 is 360 cm thick. This typical porous pale-yellow loess is intercalated by two embryonic weakly developed paleosols at approximate depths of 3.75 cm (L1LL1SSS2) and 1.75 cm (L1LL1SSS1), respectively. The top of the loess subunit L1LL1 is heavily bioturbated at the contact with the modern pedocomplex S0. This Holocene soil has a thickness of approximately 90 cm. The lower Ck horizon contains many $CaCO_3$ nodules of 1–5 cm in diameter and former root channels were infiltrated by upper humic material. The transitional AC horizon (10YR 5/1 3/3) is 15 cm thick, consisting of very porous silt loam with a granular structure. At the top, typical granular Ah horizon (10YR 6/3 4/4) remarkable krotovinas are present. Table 1 shows the detailed morphological description of the Novo Orahovo loess and paleosol units.

Table 1. Detailed morphological description of the loess–paleosol sequence at the Novo Orahovo brickyard.

Unit	Thickness (cm)	Depth (cm)	Description
L2	75	1000–925	Porous pale yellow (5YR 4/3, 5/4) typical loess with many humic infiltrations and carbonate concretions (ø 1–3 cm), intensively bioturbated.
S1	155	925–890	A basal transitional AB horizon has granular and partly platy structure (10YR 6/2–4).
		890–855	Ah1 lower humic (10YR 6/3, 4/2) horizon with granular structure, carbonate concretions (ø 1–2 cm), and krotovinas.
		855–820	Upper lighter Ah2 (10YR 5/3–4) with carbonate concretions (ø 1–2) has typical granular structure.
		820–770	The upper mollic A horizon with brighter color (10YR 6/2–4) and many carbonate pseudomycelia.
L1	680	770–515	Loess subunit L1LL2 is a porous typical loess (5YR 7/3, 5/4) intercalated by sandy layers in some parts with krotovinas.
		515–450	PaleosolL1SS1 is a fossil A horizon (10YR 4/2, 6/3) with intensive granular structure partly disturbed by krotovinas.
		450–90	Loess subunit L1LL1 I is a typical porous loess (10YR 7/4, 5/3) intercalated with two weakly developed initial paleosols, L1LL1SSS2 and L1LL1SSS1.
S0	90	90–75	Ck with many soft spherical carbonate nodules (ø 1–5 cm) intensively bioturbated with humic infiltrations and krotovinas.
		75–60	Transitional AC horizon is very porous with many carbonate pseudomycelia.
		60–0	Typical strongly developed granular Ah horizon (10YR 6/3, 4/4).

3.2. Magnetic Susceptibility (MS)

MS records within the Novo Orahovo loess–paleosol sequence mostly coincide with lithologic and pedologic variations reflecting the changes in past climate and environmental conditions. The magnetic record supports the SPECMAP marine oxygen-isotope record of the past 150,000 years [52,53].

Figure 3 shows MS records at the Novo Orahovo section. The values of MS are related to pedogenetic processes and reflect differences in composition, concentration, and particle size of magnetic minerals between interglacial, interstadial, and stadial loess

and paleosol units [54,55]. MS variations in the interglacial pedocomplexes S1 (average 60.5 SI units) and S0 (average 34.2 SI units) are higher than those measured in loess layers L2 (average 15.6 SI units), L1LL2 (average 188 SI units), and L1LL1 (average 20.8 SI units). The weakly developed interstadial fossil soil L1SS1 has relatively low MS values (average 25.6 SI units) compared to the interglacial paleosols; they are only slightly higher than the values measured in loess strata. Two initial pedogenic layers within loess unit L1LL1 are characterized by similar MS values as observed in loess deposits. The MS variations recorded at the Novo Orahovo loess–paleosol sequence generally display a great similarity to other investigated loess sections in the Vojvodina region [2,3]. This type of magnetic signal enhancement via soil formation is also similar to those observed in Chinese and Central Asian loess deposits [54–57].

3.3. Grain-Size (GS) Variations

Variations in the GS distribution in comparison to the pedostratigraphy of the Novo Orahovo loess–paleosol sequence are presented in Figure 4. Generally, the GS record at the Novo Orahovo section corresponds less to pedostratigraphy than other previously investigated sections [8,17,18]. The loess grain-size distribution shows a minor clay subfraction at all levels (e.g., samples in Figure 4 at 415 cm (L1LL1) 6.9% and 725 cm (L1LL2) 6.8% depth), while in the paleosols, a slight but distinctive increase of the clay subfraction is present: a slight increase in the weak subsoil at 565 cm in L1SS1 (e.g., Figure 5 at 565 cm depth) reaching 11%. Further along, L2 (below 950 cm) shows a high clay content of 22% (Figure 4).

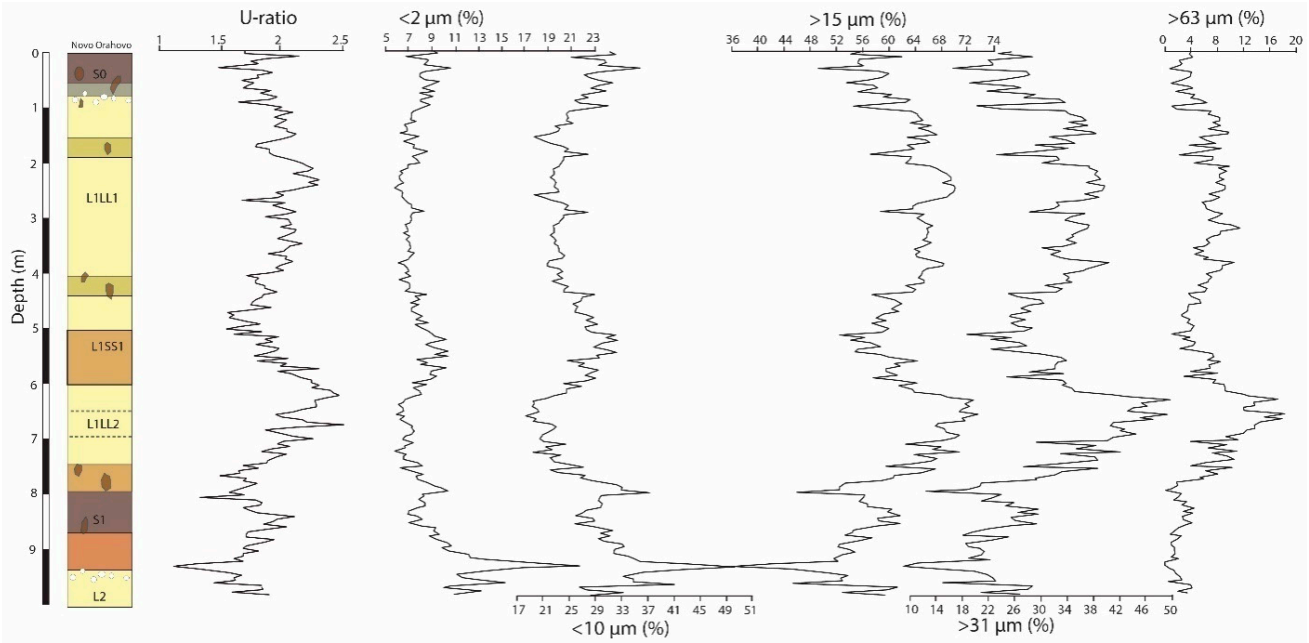

Figure 4. Grain-size variations recorded at the Novo Orahovo loess–paleosol sequence related to pedostratigraphy.

In contrast, U-values remain relatively similar in all loess units and paleosols (only a slightly smaller modal value at 965 cm). The U-ratio of the Holocene soil at the Novo Orahovo loess profile has an average value of 1.9, which was also an average value during the Early glacial. The maximum U-value of S0 is present in the first 10 cm of the profile (2.2). The average Late Pleniglacial U-ratio is slightly higher in the depth intervals of 235 cm to 265 cm and in between 600 cm and 700 cm. A slight drop of the U-ratio is present in the Middle Pleniglacial (average value of 2.2–2.5). The last interglacial phase has, on average, slightly lower values in paleosol S1. Values of the U-ratio are increasingly moving from the top of the profile towards approximately 250 cm depth, after which they decrease continuously until the base of the L1LL1 loess unit. From there, the U-ratio is steadily increasing

towards the middle part of L1LL2 and decreases again until a depth of approximately 850 cm in pedocomplex S1. The last interglacial pedocomplex, S1, is characterized by relatively high U-ratio values compared with the transition to the penultimate glacial loess unit, L2 (Figure 4).

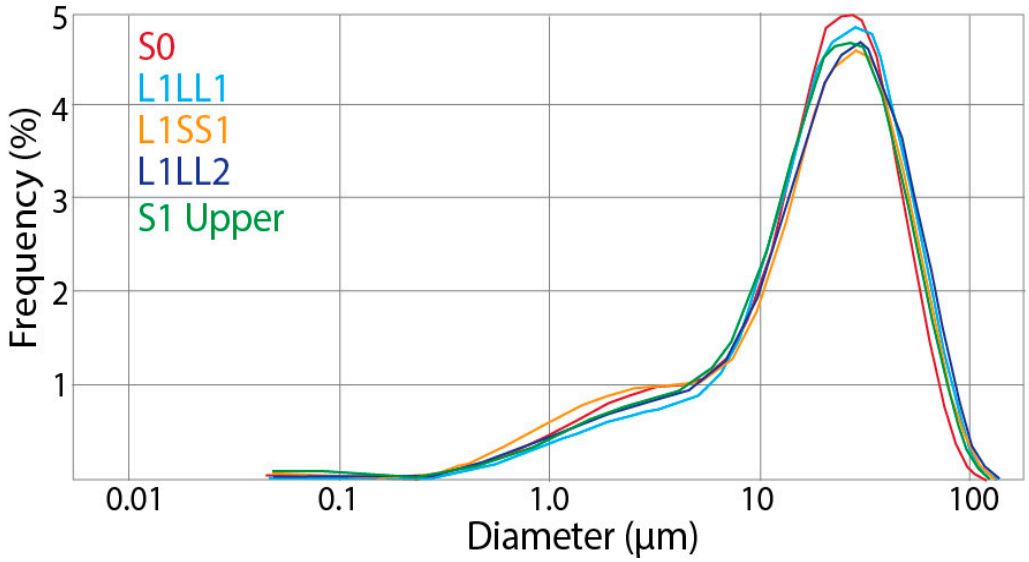

Figure 5. The frequency distributions of samples from S0, L1LL1, L1S1, L1LL2, and S1 of the Novo Orahovo loess section.

The lowest values of grain sizes <2 μm occur in the loess layers with a minimum value of 6% in L1LL1 and L1LL2. The percentage increases with pedogenesis, as the S0, L1SS1, and S1 have maximum values of 11%, 10%, and 22%, respectively. The latest value corresponds to the AB horizon of the Early glacial. The <10 μm curve is in good agreement with the <2 μm fraction, as lower values follow the Early and Late Pleniglacial with 18% and 19%, respectively. This granulation is dominant at a depth of 9.35 m, where it comprises up to 50% of the sample (this single sample might also be considered as an exceptional outlier). The Middle Pleniglacial is more pronounced with the maximum value of 32%, reaching almost the value of the Holocene soil. The next three curves of >15 μm, >31 μm, and >63 μm content display inversed values to the previous two. The maximum values of the grain-size fraction >15 μm is seen in the loess horizon L1LL2 (73%) and the minimum is at paleosol S1 (36%). The values of >31 μm fractions drop to 9%, 19%, and 17% in the soil units S1, L1SS1, and S0, respectively. Higher values are present in the glacial periods. The minimum values of the grain sizes >63 μm reach 0% in soils, while the maximum value of 18% is present in the Early Pleniglacial, indicating fine sand bands.

3.4. Luminescence Geochronology

The De value did not show any significant sensitivity to preheat temperature up to 300 °C, with the recycling ratios close to unity and the recuperation close to 1% over the 160–300 °C first preheat interval. The dose recoveries given various preheats are summarized in Figure 2a. The overall average measured-to-given-dose ratio is 1.03 ± 001 (n = 21). The results show that at any given temperature over the 160–300 °C first preheat interval, the SAR protocol was able to recover a given dose within 10% of unity. However, no clear plateau could be observed over the entire 160–300 °C preheat temperature interval. For this reason, a preheat temperature of 240 °C, which gave the best measured dose ratio, is chosen for all consecutive measurements.

Table 2 presents results for the U, Th, and K concentrations, water content, calculated total dose rates, and ages. The calculated OSL ages range from 15.9 ± 0.5 ka to 47.8 ± 1.6 ka, indicating that the upper 610 cm of the Novo Orahovo loess section formed during Marine

Isotope Stages MIS 2–MIS 4. The ages show a consistent increase and display no jumps nor inversions outside error margins. Sample 1151, taken below the boundary between S0 and L1 (110 cm depth), was dated at 15.9 ± 0.5 ka, suggesting accumulation during the late phase of MIS 2. This is consistent with other dated loess sections in the region, as similar ages of 13.6 ± 1.0 ka and 10.2 ± 0.7 ka for the upper part of L1 were reported for the Titel LP and the Irig loess site, respectively [9,58].

Table 2. Summary of sample codes, depth information, present-day water content (WC), radionuclide activities, α-values, total dose rates, weighted mean De values, and luminescence ages for the Novo Orahovo samples. Error terms are given at 1 standard error.

Scheme	Depth (cm)	WC (%)	U (ppm)	Th (ppm)	K (%)	α-Values	(Gy.ka^{-1})	De (Gy)	Age (ka)
1151	110	10.0 ± 2.0	2.80 ± 0.03	8.48 ± 0.15	1.23 ± 0.05	0.055 ± 0.003	3.00 ± 0.07	47.9 ± 0.7	15.9 ± 0.5
1147	225	12.5 ± 2.5	2.95 ± 0.03	8.70 ± 0.16	1.30 ± 0.05	0.040 ± 0.004	2.90 ± 0.07	57.7 ± 1.7	19.9 ± 0.8
1144	325	12.5 ± 2.5	2.83 ± 0.03	8.58 ± 0.15	1.27 ± 0.05	0.036 ± 0.003	2.78 ± 0.07	65.9 ± 0.8	23.8 ± 0.7
1141	435	12.5 ± 2.5	3.24 ± 0.04	10.57 ± 0.18	1.61 ± 0.06	0.030 ± 0.002	3.20 ± 0.08	86.1 ± 1.0	26.9 ± 0.7
1138	610	12.5 ± 2.5	2.66 ± 0.03	9.22 ± 0.17	1.29 ± 0.05	0.029 ± 0.002	2.64 ± 0.06	126.4 ± 3.0	47.8 ± 1.6

The sample 1147 at 225 cm depth that was recovered below the uppermost intercalated paleosol L1LL1SSS1 was dated at 19.9 ± 0.8 ka. Analogous ages were reported for the Titel LP (19.7 ± 1.7–27.8 ± 2.1 ka) by Perić et al. (2019) [9] for the L1 loess at depths 209–227 cm. The OSL age for sample 1144 taken from the central part of L1 (325 cm depth) was 23.8 ± 0.7 ka. The underlying sample 1141 recovered from L1LL1SSS2 was dated at 26.9 ± 0.7 ka, suggesting it developed shortly after the transition between MIS 2 and MIS 3. Schmidt et al. (2010) [59] and Murray et al. (2014) [60] also reported comparative ages of 23.3 ± 1.5 and 23.6 ± 1.4 ka, respectively, for the L1L1 loess at the Stari Slankamen section. The lowermost sample 1138 taken at the L1S1L1LL2 boundary yielded an age of 47.8 ± 1.6 ka. This suggests that the formation of the L1SS1 paleosol started somewhat later in MIS 3 and fits with the expected age for this paleosol layer. Most recently, similar ages for the L1S1SS1 paleosol (27–38 ka) were observed at the Irig loess–paleosol sequence [57]. Comparable ages for the upper paleosols in the Vojvodina region have also been reported for numerous loess sites: Surduk: 31.8 ± 3.7 ka [61], Stari Slankamen: 34.4 ± 2.2 ka [59], Crvenka: 38 ± 4 ka [6], and the Titel LP: 34.2 ± 2.4 ka [9].

As demonstrated above, the calculated OSL ages for the upper 610 cm for the Novo Orahovo loess profile show a remarkable agreement with the ages from several investigated loess–paleosol sequences in the Vojvodina region. This implies that the loess accumulation and paleosol formation had a similar trend in this region.

4. Discussion

The Novo Orahovo loess site is located further to the northeast compared to other similar previously investigated Northern Serbian loess sections. Figure 6 shows the relationship between low-field MS records of investigated loess sites in Vojvodina and their correlation with the marine oxygen-isotope stratigraphy [62]. Variations in MS correlate closely with the pedostratigraphy of the analyzed exposures, providing a similar pattern of variation, and the main MS peaks can be easily correlated between the sections. The general pattern of magnetic records of Irig, Ruma, Batajnica, Stari Slankamen, Mošorin (Titel loess plateau), Crvenka, and Novo Orahovo sections is characterized by high MS values in strongly developed interglacial soils S0 and S1, low MS values in loess layers L1LL1, L1LL2, and L2, and slightly higher values in weakly developed and morphologically variable L1SS1 pedocomplex.

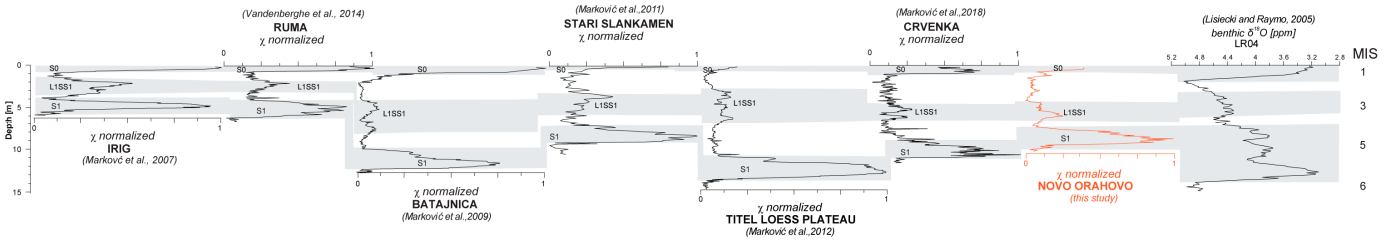

Figure 6. Relationship between low-field MS normalized records of loess–paleosol sequences Irig (Markovic et al., 2007) [19], Ruma (Vandenberghe et al., 2014) [8], Stari Slankamen (Marković et al., 2011) [63], Batajnica (Marković et al., 2009) [64], Titel loess plateau (Marković et al., 2012) [65], and Crvenka (Marković et al., 2018) [22] in the Vojvodina region and the Novo Orahovo loess sequence plotted on a depth scale. They are correlated with the LR04 paleoclimatic stack model of Lisiecki and Raymo (2005) [66].

The geographical position of the Novo Orahovo site provides a unique opportunity to reconstruct climate and environmental evolution in the transitional area between the south-eastern limit and central part of the Carpathian (Pannonian) Basin. While the paleoclimatic and paleoenvironmental reconstruction derived from the loess–paleosol sequences at the Novo Orahovo brickyard generally displays a similar stratigraphic pattern and magnetic variations observed in other investigated sites in the Vojvodina region [2,3] (Figure 6), there are also some distinct differences in glacial–interglacial GS distributions compared to other similar sites in the region. For example, at the Novo Orahovo section, the Middle Pleniglacial warm climatic conditions are reflected in an increase of MS values in weakly developed pedocomplex L1SS1. Compared to this, higher MS values in the upper part of pedocomplex L1SS1 are observed at the Irig, Ruma, Batajnica, and Stari Slankamen sections situated at the Srem LP. The MS pattern of the Veliki Surduk section at Titel LP and Crvenka at the southern limit of Bačka LP, located in between the Srem loess plateau and the Novo Orahovo section, show more uniform values. Further investigations will need to be tailored to address the question: do these changes in MS variations represent regional paleoclimatic gradient or is this just a consequence of some local environmental exception related to the Novo Orahovo loess–paleosol sequence? The mean grain size at Novo Orahovo is slightly coarser than in other sections in Vojvodina. The modal values at Novo Orahovo are 29–37 μm from the top to the bottom of S1. At Irig, the mode is 22–32 μm (except two samples in the L1LL1 loess unit) [58], while at Ruma [8], the mode is 24–29 μm. It is not likely that the wind strength increases would be equal in both glacial and interglacial periods at Novo Orahovo in contrast to other places in the Vojvodina region and also in China (e.g., the Luochuan type loess site [8]). Therefore, the grain size of the source region may be the reason for these conditions. Additionally, loess and paleosol units between Irig and Ruma show variable morphological characteristics of recent and two younger fossil soils (L1SS1 and S1). Vandenberghe et al. (2014) [8] interpreted these geomorphological forms as relicts of dry valleys (dels) which potentially served as local sources for loess transport. Ludwig et al. (2021) [61] found that in the Carpathian Basin during the Last Glacial Maximum peak, dust emissions in spring coincide with the highest wind speeds and relatively low precipitation amounts.

The similarity between the modal values and U-ratios of loess and paleosols at Novo Orahovo supports the idea that loess deposition was restricted or absent during interglacials, as was also demonstrated at the Ruma loess site [8]. Since U-values, displaying grain sizes >5 μm, reflect the dust properties, the general stability of U-values in both loess and paleosols point to a similar source area and transport process in loess as well as in paleosols.

The U-ratios in the Novo Orahovo section are between 1.1 in paleosol layers and 2.5 in loess units. These values are generally similar to other Serbian loess sites such as Ruma (U-ratio varying between 1.6 and 2.2) [8], Irig (U-ratio varying between 1.4 and 2.0) [10], and Dupljaja (U-ratio varying between 1.4 and 2.1), as well as in the famous Chinese type

loess section in Luochuan, with a U-ratio that varies between 1.0 and 2.2 [8,51]. The stability and relatively high values of the modal size at Novo Orahovo contrast with many sites in plateau position in the Vojvodina region [2,5,49,60,67] and China [51].

Novo Orahovo's geomorphological position provides a reasonable explanation for the described regional variability in grain-size records. The site is located near the Čik River valley, and also in the vicinity of recent and paleo-floodplains of the Tisza and Mures rivers to the east, as well as the dune fields to the north, as potential sources of aeolian material (Figure 1). We conclude that the regional geomorphological position of the site—more specifically, the relative distance to source areas for loess supply—provides a good explanation for the regional differences of dustiness, as expressed by loess accumulation rate and grain-size variability (especially the modal size) of the loess cover. This is in agreement with the conclusions by Stevens et al. (2020) in England [68].

Finally, Novo Orahovois is located in the modern, most arid, part of the Carpathian Basin (Figure 7A). Gavrilov et al. (2021) [69] provided a map of spatial distribution of aridity (the De Martonne Aridity Index) based on data from 78 meteorological stations in Hungary and Vojvodina during the period between 1949 and 2017. Aridity is most pronounced during the summer season (Figure 7B). Several previous studies have suggested that current climatic gradients in the region are similar to those during the Late Pleistocene period [2,3,15–17,66]. These arid local climate conditions associated with sparse vegetation make the surroundings of Novo Orahovo sensitive to the emission of material available for further aeolian action. Biotic proxy records from other Bačka LP sites, such as Madaras [70–72], Katymár [70–74], and Crvenka [6,21,22], also support previous interpretations. A novel n-alkenes paleoenvironmental record provides evidence for the continued dominance of grasslands during the Late Pleistocene at the Crvenka loess site, indicating more arid climate during the interglacial than glacial periods [6,21,22]. In spite of the general predomination of different grassland environments at Bačka LP, analyzed biotic proxies also show that stadials were more humid than interstadials, leading to the expansion of arboreal plants influencing reduced erosion and aeolian input in cooler phases [6,21,22,71–74].

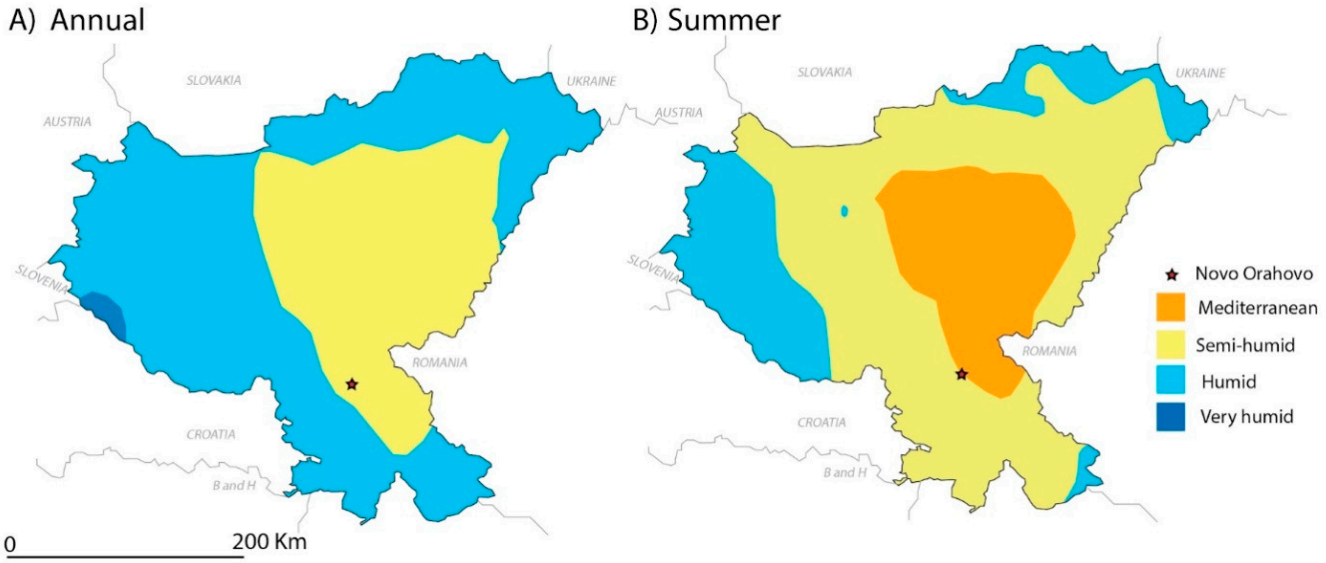

Figure 7. The spatial distribution of the De Martonne Aridity Index for Hungary and Vojvodina jointly during the period 1949–2017: (**A**) annual, (**B**) summer (Gavrilov et al., 2021, modified) [69]. The star symbol indicates the position of the Novo Orahovo loess site.

5. Conclusions

Investigations of the loess–paleosol sequence at the Novo Orahovo brickyard have established the importance of this site as a record of Late Pleistocene climate and environmental dynamics in the southeastern part of the Carpathian Basin.

The loess record at Novo Orahovo provides an opportunity to reconstruct local and regional environmental processes and conditions during the past ∼150,000 years. Sedimentological, pedological, and magnetic evidence recorded in Novo Orahovo show many similarities with previously investigated loess sites in the Vojvodina region, indicating relatively stable Late Pleistocene environmental conditions at these discontinuous loess plateaus. However, the observed specific grain-size composition of the Novo Orahovo loess–paleosol sequence is a consequence of its specific geomorphological position and most likely existence of arid climate conditions. These environmental conditions promote higher availability of the source material for further aeolian action. Additionally, existing biotic proxies from other investigated sites at Bačka LP indicate the standing of favorable local vegetation conditions for dust uptake during the whole Late Pleistocene.

Author Contributions: Conceptualization, S.B.M., J.V., Z.M.P. and G.S.; Methodology, G.S., Z.M.P., M.G.R. and J.V.; validation, S.B.M., J.V., Q.H., T.L., N.T., A.A., T.L. and I.C.; formal analysis, D.F., T.B., Z.M.P. and R.S.M.; investigation, S.B.M., G.S., N.T. and R.S.M.; writing—original draft preparation, S.B.M., J.V. and G.S.; writing—review and editing, M.B.G., I.C., N.T. and Q.H.; visualization, M.G.R., S.B.M., A.A., J.V. and R.S.M. All authors have read and agreed to the published version of the manuscript.

Funding: This research was supported by Project F-178 of the Serbian Academy of Sciences and Arts. The authors gratefully acknowledge the financial support of the Ministry of Science, Technological Development and Innovation of the Republic of Serbia (Grant No. 451-03-47/2023-01/200125) and grant F-178 of the Serbian Academy of Sciences and Arts. I.C. was supported by La Caixa Junior Leader Grant 2020 (Marie Skłodowska-Curie grant agreement No 847648).

Institutional Review Board Statement: Not applicable.

Informed Consent Statement: Not applicable.

Data Availability Statement: Not applicable.

Acknowledgments: We wish to thank the Novo Orahovo brick factory for allowing the team to work in the quarry. We are very grateful to three anonymous reviewers for constructive suggestions and comments.

Conflicts of Interest: Author Aleksandar Antić is an employee of MDPI; however, he was not working for the journal *Quaternary* at the time of submission and publication.

References

1. Bronger, A. Correlation of loess–paleosol sequences in East and Central Asia with SE Central Europe: Towards a continental Quaternary pedostratigraphy and paleoclimatic history. *Quat. Int.* **2002**, *106–107*, 11–31. [CrossRef]
2. Marković, S.B.; Bokhorst, M.P.; Vandenberghe, J.; McCoy, W.D.; Oches, E.A.; Hambach, U.; Gaudenyi, T.; Jovanović, M.; Zöller, L.; Stevens, T.; et al. Late Pleistocene loess-palaeosol sequences in the Vojvodina region, north Serbia. *J. Quat. Sci.* **2008**, *23*, 73–84. [CrossRef]
3. Marković, S.B.; Stevens, T.; Kukla, G.J.; Hambach, U.; Fitzsimmons, K.E.; Gibbard, P.; Buggle, B.; Zech, M.; Guo, Z.; Hao, Q.; et al. Danube loess stratigraphy—Towards a pan-European loess stratigraphic model. *Earth-Sci. Rev.* **2015**, *148*, 228–258. [CrossRef]
4. Antoine, P.; Rousseau, D.D.; Lautridou, J.P.; Hatté, C. Last interglacial-glacial climatic cycle in loess-paleosol successions of north-western France. *Boreas* **1999**, *28*, 551–563. [CrossRef]
5. Bokhorst, M.P.; Beets, C.J.; Marković, S.B.; Gerasimenko, N.P.; Matviishina, Z.N.; Frechen, M. Pedo-chemical climate proxies in Late Pleistocene Serbian–Ukranian loess sequences. *Quat. Int.* **2009**, *198*, 113–123. [CrossRef]
6. Stevens, T.; Marković, S.B.; Zech, M.; Hambach, U.; Sümegi, P. Dust deposition and climate in the Carpathian Basin over an independently dated last glacial-interglacial cycle. *Quat. Sci. Rev.* **2011**, *30*, 662–681. [CrossRef]
7. Zech, R.; Zech, M.; Marković, S.; Hambach, U.; Huang, Y. Humid glacials, arid interglacials? Critical thoughts on pedogenesis and paleoclimate based on multi-proxy analyses of the loess-paleosol sequence Crvenka, Northern Serbia. *Palaeogeogr. Palaeoclimatol. Palaeoecol.* **2013**, *387*, 165–175. [CrossRef]

8. Vandenberghe, J.; Marković, S.B.; Jovanović, M.; Hambach, U. Site-specific variability of loess and palaeosols (Ruma, Vojvodina, northern Serbia). *Quaternery Int.* **2014**, *334–335*, 86–93. [CrossRef]
9. Perić, Z.; LagerbäckAdolphi, E.; Stevens, T.; Újvári, G.; Zeeden, C.; Buylaert, J.P.; Marković, S.B.; Hambach, U.; Fischer, P.; Schmidt, C.; et al. Quartz OSL dating of late quaternary Chinese and Serbian loess: A cross Eurasian comparison of dust mass accumulation rates. *Quat. Int.* **2019**, *502*, 30–44. [CrossRef]
10. Lehmkuhl, F.; Bösken, J.; Hošek, J.; Sprafke, T.; Marković, S.B.; Obreht, I.; Hambach, U.; Sümegi, P.; Thiemann, A.; Steffens, S.; et al. Loess distribution and related Quaternary sediments in the Carpathian Basin. *J. Maps* **2018**, *14*, 661–670. [CrossRef]
11. EORC, J. ALOS Global Digital Surface Model "ALOS World 3D-30m"(AW3D30). 2016. Available online: http://www.eorc.jaxa.jp/ALOS/en/aw3d30/index.htm (accessed on 6 August 2020).
12. Perić, Z.M.; Marković, S.B.; Sipos, G.; Gavrilov, M.B.; Thiel, C.; Zeeden, C.; Murray, A.S. A post-IR IRSL chronology and dust mass accumulation rates of the Nosak loess-palaeosol sequence in north-eastern Serbia. *Boreas* **2020**, *49*, 841–857. [CrossRef]
13. Fenn, K.; Durcan, J.A.; Thomas, D.S.G.; Banak, A. A 180 ka record of environmental change at Erdut (Croatia): A new chronology for the loess–palaeosol sequence and its implications for environmental interpretation. *J. Quat. Sci.* **2020**, *35*, 582–593. [CrossRef]
14. Pötter, S.; Veres, D.; Baykal, Y.; Nett, J.J.; Schulte, P.; Hambach, U.; Lehmkuhl, F. Disentangling sedimentary pathways for the Pleniglacial Lower Danube loess based on geochemical signatures. *Front. Earth Sci.* **2021**, *9*, 600010. [CrossRef]
15. Sümegi, P.; Gulyás, S. Some notes on the interpretation and reliability of malacological proxies in paleotemperature reconstructions from loess-comments to Obreht et al.'s "A critical reevaluation of paleoclimate proxy records from loess in the Carpathian Basin". *Earth-Sci. Rev.* **2021**, *221*, 103675. [CrossRef]
16. Laag, C.; Hambach, U.; Zeeden, C.; Lagroix, F.; Guyodo, Y.; Veres, D.; Jovanović, M.; Marković, S.B. A detailed paleoclimate proxy record for the Middle Danube Basin over the last 430 kyr: A rock magnetic and colorimetric study of the Zemun loess-paleosol sequence. *Front. Earth Sci.* **2021**, *9*, 600086. [CrossRef]
17. Marković, S.B.; Oches, E.A.; Sümegi, P.; Jovanović, M.; Gaudenyi, T. An introduction to the Middle and Upper Pleistocene loess–paleosol sequences at Ruma Brickyard (Vojvodina, Yugoslavia). *Quat. Int.* **2006**, *149*, 80–86. [CrossRef]
18. Marković, S.B.; McCoy, W.D.; Oches, E.A.; Savić, S.; Gaudenyi, T.; Jovanović, M.; Stevens, T.; Walther, R.; Ivanišević, P.; Galić, Z. Paleoclimate record in the Late Pleistocene loess-paleosol sequence at Petrovaradin Brickyard (Vojvodina, Serbia). *GeologicaCarpathica* **2005**, *56*, 545–552.
19. Marković, S.B.; Oches, E.A.; McCoy, W.D.; Frechen, M.; Gaudenyi, T. Malacological and sedimentological evidence for "warm" glacial climate from the Irig loess sequence, Vojvodina. Serbia. *Geochem. Geophys. Geosyst.* **2007**, *8*, Q09008. [CrossRef]
20. Marković, S.B.; Oches, E.A.; Perić, Z.M.; Gaudenyi, T.; Jovanović, M.; Sipos, G.; Thiel, C.; Buylaert, J.; Savić, S.; McCoy, W.D.; et al. The Požarevac loess–paleosol sequence: A record of increased aridity in the south-eastern margin of the Carpathian Basin during the last 350 ka. *J. Quat. Sci.* **2021**, *36*, 1436–1447. [CrossRef]
21. Sümegi, P.; Marković, S.B.; Molnár, D.; Sávai, S.; Náfrádi, K.; Szelepcsényi, Z.; Novák, Z. Črvenka loess-paleosol sequence revisited: Local and regional Quaternary biogeographical inferences of the southern Carpathian Basin. *Open Geosci.* **2016**, *8*, 390–404. [CrossRef]
22. Marković, S.B.; Sümegi, P.; Stevens, T.; Schaetzl, R.J.; Obreht, I.; Chu, W.; Buggle, B.; Zech, M.; Zech, R.; Zeeden, C.; et al. The Crvenka loess-paleosol sequence: A record of continuous grassland domination in the southern Carpathian Basin during the Late Pleistocene. *Palaeogeogr. Palaeoclim. Palaeoecol.* **2018**, *509*, 33–46. [CrossRef]
23. Chen, H.; Shao, M.; Li, Y. Soil desiccation in the Loess Plateau of China. *Geoderma* **2008**, *143*, 91–100. [CrossRef]
24. Vandenberghe, J.; Hujizer, B.; Mücher, H.; Laan, W. Short climatic oscillations in a western European loess sequence (Kesselt, Belgium). *J. Quat. Sci.* **1998**, *13*, 35–38. [CrossRef]
25. Antoine, P.; Rousseau, D.D.; Zöller, L.; Lang, A.; Munaut, A.V.; Hatté, C.; Fontugne, M. High resolution record of the last interglacial-glacial cycle in loess palaeosol sequences of Nussloch (Rhine Valley–Germany). *Quat. Int.* **2001**, *76/77*, 211–229. [CrossRef]
26. Rousseau, D.D.; Zöller, L.; Valet, J.P. Climatic variations in the Upper Pleistocene loess sequence at Achenheim (Alsace, France): Analysis of magnetic susceptibility and thermoluminescence chronology. *Quat. Res.* **1998**, *49*, 255–263. [CrossRef]
27. Rousseau, D.D.; Gerasimenko, N.; Matvviishina, Z.; Kukla, G.J. Late Pleistocene environments of central Ukraine. *Quat. Res.* **2001**, *56*, 349–356. [CrossRef]
28. Rousseau, D.D.; Antoine, P.; Christine, H.; Lang, A. Abrupt millennial climatic changes from Nussloch (Germany) Upper Weichselianeolian records during the last glaciation. *Quat. Sci. Rev.* **2002**, *21*, 1577–1582. [CrossRef]
29. Jary, Z. Periglacial markers within the Late Pleistocene loess–palaeosol sequences in Poland and Western Ukraine. *Quat. Int.* **2009**, *198*, 124–135. [CrossRef]
30. Moine, O.; Rousseau, D.-D.; Antoine, P. The impact of Dansgaard–Oeschger cycles on the loessic environment and malacofauna of Nussloch (Germany) during the Upper Weichselian. *Quat. Res.* **2008**, *70*, 91–104. [CrossRef]
31. Lehmkuhl, F.; Nett, J.J.; Potter, S.; Schulte, P.; Sprafke, T.; Jary, Z.; Antoine, P.; Wacha, L.; Wolf, D.; Zerboni, A.; et al. Loess landscapes of Europe—Mapping, geomorphology, and zonal differentiation. *Earth-Sci. Rev.* **2021**, *215*, 103769. [CrossRef]
32. Kun, Á.; Katona, O.; Sipos, G.; Barta, K. Comparison of Pipette and Laser Diffraction Methods in Determining the Granulometric Content of Fluvial Sediment Samples. *J. Environ. Geogr.* **2013**, *6*, 49–54. [CrossRef]

33. Serban, R.D.; Sipos, G.; Popescu, M.; Urdea, P.; Onaca, A.; Ladányi, Z. Comparative Grain-Size Measurements for Validating Sampling and Pretreatment Techniques in Terms of Solifluction Landforms, Southern Carpathians, Romania. *J. Environ. Geogr.* **2015**, *8*, 39–47. [CrossRef]
34. Sipos, G.; Marković, S.B.; Gavrilov, M.B.; Balla, A.; Filyó, D.; Bartyik, T.; Mészáros, M.; Tóth, O.; van Leeuwen, B.; Lukić, T.; et al. Late Pleistocene and Holocene aeolian activity in the Deliblato Sands, Serbia. *Quat. Res.* **2022**, *107*, 113–124. [CrossRef]
35. Vandenberghe, J.; Roebroeks, W.; Gemke, D. Lithostratigraphy and palaeoenvironment of the Pleistocene deposits at Maastricht-Belvédère, southern Limburg, the Netherlands. *Analecta Praehist. Maastricht-BelvÈdËre Stratigr. Palaeoenvironment Archaeol. Middle Late Pleistocenedeposits* **1985**, *18*, 7–18.
36. Mauz, B.; Bode, T.; Mainz, E.; Blanchard, H.; Hilger, W.; Dikau, R.; Zöller, L. The luminescence dating laboratory at the University of Bonn: Equipment and procedures. *Anc. TL* **2002**, *20*, 53–61.
37. Bøtter-Jensen, L.; Thomsen, K.; Jain, M. Review of optically stimulated luminescence (OSL) instrumental developments for retrospective dosimetry. *Radiat. Meas.* **2010**, *45*, 253–257. [CrossRef]
38. Murray, A.S.; Wintle, A.G. The single aliquot regenerative dose protocol: Potential for improvements in reliability. *Radiat. Meas.* **2003**, *37*, 377–381. [CrossRef]
39. Wintle, A.; Murray, A. A review of quartz optically stimulated luminescence characteristics and their relevance in single-aliquot regeneration dating protocols. *Radiat. Meas.* **2006**, *41*, 369–391. [CrossRef]
40. Duller, G.A.T. Distinguishing quartz and feldspar in single grain luminescence measurements. *Radiat. Meas.* **2003**, *37*, 161–165. [CrossRef]
41. Mauz, B.; Packman, S.; Lang, A. The alpha effectiveness in silt-sized quartz: New data obtained by single and multiple aliquot protocols. *Anc. TL* **2006**, *24*, 47–52.
42. Liritzis, I.; Vafiadou, A.; Zacharias, N.; Polymeris, G.S.; Bednarik, R.G. Advances in surface luminescence dating: New data from selected monuments. *Mediterr. Archaeol. Archaeom.* **2013**, *13*, 105–115.
43. Brennen, G.K.; Caves, C.M.; Jessen, P.S.; Deutsch, I.H. Quantum Logic Gates in Optical Lattices. *Phys. Rev. Lett.* **1999**, *82*, 1060–1063. [CrossRef]
44. Brennan, J.D. Preparation and Entrapment of Fluorescently Labeled Proteins for the Development of Reagentless Optical Biosensors. *J. Fluoresc.* **1999**, *9*, 295–312. [CrossRef]
45. Guérin, G.; Mercier, N.; Adamiec, G. Dose-rate conversion factors: Update. *Anc. TL* **2011**, *29*, 5–8.
46. Prescott, J.; Hutton, J. Cosmic ray contributions to dose rates for luminescence and ESR dating: Large depths and long-term time variations. *Radiat. Meas.* **1994**, *23*, 497–500. [CrossRef]
47. Durcan, J.A.; King, G.E.; Duller, G.A. DRAC: Dose Rate and Age Calculator for trapped charge dating. *Quat. Geochronol.* **2015**, *28*, 54–61. [CrossRef]
48. Liu, T.S. *The Loess Deposits of China*; Science Press: Beijing, China, 1965. (In Chinese)
49. Kukla, G. Loess stratigraphy in central China. *Quat. Sci. Rev.* **1987**, *6*, 191–219. [CrossRef]
50. Kukla, G.; An, Z. Loess stratigraphy in Central China. *Palaeogeogr. Palaeoclim. Palaeoecol.* **1989**, *72*, 203–225. [CrossRef]
51. Vandenberghe, J.; Zhisheng, A.; Nugteren, G.; Huayu, L.; Van Huissteden, K. New absolute time scale for the Quaternary climate in the Chinese Loess region by grain-size analysis. *Geology* **1997**, *25*, 35–38. [CrossRef]
52. Bassinot, F.C.; Labeyrie, L.D.; Vincent, E.; Quidelleur, X.; Shackleton, N.J.; Lancelot, Y. The astronomical theory of climate and the age of the Brunhes-Matuyama magnetic reversal. *Earth Planet. Sci. Lett.* **1994**, *126*, 91–108. [CrossRef]
53. Martinson, D.; Pisias, M.G.; Hays, J.D.; Imbrie, J.; Moore, T.C.; Shackleton, N.J. Age dating and the orbitaltheory of ice ages: Development of a high-resolution 0 to300,000-year chronostratigraphy. *Quat. Res.* **1987**, *27*, 1–30. [CrossRef]
54. Heller, F.; Evans, M.E. Loess magnetism. *Rev. Geophys.* **1995**, *33*, 211–240. [CrossRef]
55. Maher, B.A. Magnetic properties of modern soils and Quaternary loessicpaleosols: Paleoclimatic implications. *Palaeogeogr. Palaeoclimatol. Palaeoecol.* **1998**, *137*, 25–54. [CrossRef]
56. Heller, F.; Liu, T.S. Paleoclimatic and sedimentary history from magnetic susceptibility of loess in China. *Geophys. Res. Lett.* **1986**, *13*, 1169–1172. [CrossRef]
57. Maher, B.A.; Thompson, R. Mineral magnetic record of the Chinese loess and paleosols. *Geology* **1991**, *19*, 3–6. [CrossRef]
58. Perić, Z.M.; Stevens, T.; Obreht, I.; Hambach, U.; Lehmkuhl, F.; Marković, S.B. Detailed luminescence dating of dust mass accumulation rates over the last two glacial-interglacial cycles from the Irig loess-palaeosol sequence, Carpathian Basin. *Glob. Planet. Change* **2022**, *215*, 103895. [CrossRef]
59. Schmidt, E.D.; Machalett, B.; Marković, S.B.; Tsukamoto, S.; Frechen, M. Luminescence chronology of the upper part of the Stari Slankamen loess sequence (Vojvodina, Serbia). *Quat. Geochronol.* **2010**, *5*, 137–142. [CrossRef]
60. Murray, A.S.; Schmidt, E.D.; Stevens, T.; Buylaert, J.P.; Marković, S.B.; Tsukamoto, S.; Frechen, M. Dating Middle Pleistocene loess from StariSlankamen (Vojvodina, Serbia)—Limitations imposed by the saturation behaviour of an elevated temperature IRSL signal. *Catena* **2014**, *117*, 34–42. [CrossRef]
61. Ludwig, P.; Gavrilov, M.B.; Marković, S.B.; Ujvari, G.; Lehmkuhl, F. Simulated regional dust cycle in the Carpathian Basin and the Adriatic Sea region during the Last Glacial Maximum. *Quat. Int.* **2021**, *581–582*, 114–127. [CrossRef]
62. Fuchs, M.; Rousseau, D.D.; Antoine, P.; Hatté, C.; Gauthier, C.; Marković, S.; Zoeller, L. Chronology of the last climatic cycle (Upper Pleistocene) of the Surduk loess sequence, Vojvodina, Serbia. *Boreas* **2008**, *37*, 66–73. [CrossRef]

63. Marković, S.B.; Hambach, U.; Stevens, T.; Kukla, G.J.; Heller, F.; William, D.; McCoy, W.D.; Oches, E.A.; Buggle, B.; Zöller, L. The last million years recorded at the Stari Slankamen loess-palaeosol sequence: Revised chronostratigraphy and long-term environmental trends. *Quat. Sci. Rev.* **2011**, *30*, 1142–1154. [CrossRef]
64. Marković, S.B.; Hambach, U.; Catto, N.; Jovanović, M.; Buggle, B.; Machalett, B.; Zöller, L.; Glaser, B.; Frechen, M. The middle and late Pleistocene loess-paleosol sequences at Batajanica, Vojvodina, Serbia. *Quat. Int.* **2009**, *198*, 255–266. [CrossRef]
65. Marković, S.B.; Hambach, U.; Jovanović, M.; Stevens, T.; O'Hara-Dhand, K.; Basarin, B.; Smalley, I.J.; Buggle, B.; Zech, M.; Svirčev, Z.; et al. Loess in Vojvodina region (Northern Serbia): The missing link between European and Asian Pleistocene environments. *Neth. J. Geosci.* **2012**, *91*, 173–188. [CrossRef]
66. Lisiecki, L.E.; Raymo, M.E. A Pliocene-Pleistocene stack of 57 globally distributed benthic δ 18O records. *Paleoceanography* **2005**, *20*, PA1003. [CrossRef]
67. Bokhorst, M.P.; Vandenberghe, J.; Sümegi, P.; Łanczont, M.; Gerasimenko, N.P.; Matviishina, Z.N.; Marković, S.B.; Frechen, M. Atmospheric circulation patterns in central and eastern Europe during the Weichselian Pleniglacial inferred from loess grain-size records. *Quat. Int.* **2011**, *234*, 62–74. [CrossRef]
68. Stevens, T.; Sechi, D.; Bradák, B.; Orbe, R.; Baykal, Y.; Cossu, G.; Tziavaras, C.; Andreucci, S.; Pascucci, V. Abrupt last glacial dust fall over southeast England associated with dynamics of the British-Irish ice sheet. *Quat. Sci. Rev.* **2020**, *250*, 106641. [CrossRef]
69. Gavrilov, M.B.; Radaković, M.G.; Sipos, G.; Mezősi, G.; Gavrilov, G.; Lukić, T.; Basarin, B.; Benyhe, B.; Fiala, K.; Kozák, P.; et al. Aridity in the Central and Southern Pannonian Basin. *Atmosphere* **2020**, *11*, 1269. [CrossRef]
70. Sümegi, P.; Krolopp, E. Quatermalacological analysis for modeling of the Upper Weichselianpalaeoenvironmental changes in the Carpathian Basin. *Quat. Int.* **2002**, *91*, 53–63. [CrossRef]
71. Molnár, D.; Sümegi, P.; Fekete, I.; Makó, L.; Sümegi, B.P. Radiocarbon dated malacological records of two Late Pleistocene loess-paleosol sequences from SW-Hungary: Paleoecological inferences. *Quat. Int.* **2019**, *504*, 108–117. [CrossRef]
72. Sümegi, P.; Gulyás, S.; Molnár, D.; Bozsó, G.; Fekete, I.; Makó, L.; Cseh, P.; Molnár, M.; Sümegi, B.P.; Almond, P.; et al. New chronology and extended palaeoenvironmental data to the 1975 loess profile of Madaras brickyard, South Hungary. *J. Quat. Sci.* **2021**, *36*, 1364–1381. [CrossRef]
73. Sümegi, P.; Molnár, D.; Gulyás, S.; Stevens, T.; Makó, L.; Cseh, P.; Molnár, M.; Fitzsimmons, K.; Nett, J.J.; Hlavatskyi, D.; et al. Comparison of High-Resolution ^{14}C and Luminescence-Based Chronologies of the MIS 2 Madaras Loess/Paleosol Sequence, Hungary: Implications for Chronological Studies. *Quaternary* **2022**, *5*, 47. [CrossRef]
74. Sümegi, P.; Molnár, D.; Gulyás, S.; Náfrádi, K.; Sümegi, B.P.; Törőcsik, T.; Persaits, G.; Molnár, M.; Vandenberghe, J.; Zhou, L. High-resolution proxy record of the environmental response to climatic variations during transition MIS3/MIS2 and MIS2 in Central Europe: The loess-paleosol sequence of Katymár brickyard (Hungary). *Quat. Int.* **2019**, *504*, 40–55. [CrossRef]